SAE INTERNATIONAL

Analysis of Cylinder Pressure Measurement Accuracy for Internal Combustion Engine Control

2017-01-1067

Published 03/28/2017

Xiaoguo Storm, Heikki J. Salminen, Reino Virrankoski, and Seppo Niemi
University of Vaasa

Jari Hyvonen
Wartsila Finland Oy

CITATION: Storm, X., Salminen, H., Virrankoski, R., Niemi, S. et al., "Analysis of Cylinder Pressure Measurement Accuracy for Internal Combustion Engine Control," SAE Technical Paper 2017-01-1067, 2017, doi:10.4271/2017-01-1067.

Abstract

With the tightening requirements on engine emission and performance, pressure based combustion controls are becoming common in medium speed large bore reciprocating internal combustion engines. The accuracy of the cylinder pressure data including the raw pressure value at its corresponding crank angle, has a vital impact on engine controllability. For instance, this work shows that a 1-bar pressure offset leads to a 0.6% variation in the total heat release (THR) while the 50% heat release crank angle (CA50) can be shifted by 1.5 degrees. Similarly, with a single degree error in the crank position, the indicated mean effective pressure (IMEP) gets a 1.8 bar error. Thus, in this work the typical errors for cylinder pressure measurement are reviewed and analyzed for large bore four stroke marine and power plant production engines.

The main sources of error for pressure measurement are thermal shock and installation defects. Meanwhile, calibration is carried out for ten production pressure transducers to provide a general accuracy result of the pressure transducers that are used in production engines.

The main sources of error for crank angle position monitoring - when done with a flywheel-based inductive system, manufacturing tolerance, installation, and the relative displacement between the pickups and the shaft due to shaft bending, shaft longitudinal movement, torsional vibration and engine block vibration are the main sources of error.

In this paper, those errors are quantified individually through simulation and their impacts on IMEP and CA50 are also presented. At last, cylinder volume deformation and its impact on combustion diagnostics are also estimated. From the result it is concluded that torsional vibration and cylinder volume deformation have the most significant effects for combustion analysis.

Introduction

The cylinder pressure signal provides a valuable source of information for engine monitoring, diagnostics and control because it is a direct feedback from the combustion status [1] [2]. With the toughening requirements on engine emission and performance, pressure-based combustion control systems have been regarded as the potential gain for the future engine, which relies mostly on pressure-extracted information such as IMEP, heat release rate, combustion duration, compression condition etc. In order to guarantee the precision of the extracted parameters, both the pressure and crank angle need to be measured with a high accuracy.

Cylinder pressure transducers have been used in research for decades, however, since recent years they are widely used in production applications due to the decreasing price of piezoelectric pressure transducers. Piezoelectric pressure transducers have various advantages that make them suitable for production applications, such as long lifetime, high natural frequency, and low price. However, there are some sources of error which impact the pressure measurement accuracy [3]:

- The piezoelectric pressure transducer is sensitive to temperature which can cause thermal shock, signal drift and sensitivity variation.
- The installation of the transducer has an effect on the accuracy of the measurement because of the location and mounting method.

On top of obtaining high accuracy cylinder pressure measurement data, there are higher requirements for a precise crank angle or cylinder volume measurement for thermodynamic analysis. There are two different methods to measure the crank angle: a crank angle encoder and a teethed/slotted wheel. Literature claims that the most

accurate method to measure cylinder pressure is to use a crank angle encoder as a trigger source to guarantee that each pressure is measured at a predefined crank angle. Although this solution shows high angular accuracy, it cannot be applied in production because of the practical and price restrictions, and reliability reasons. Thus, wheel-based solutions are commonly used in production applications.

Inductive crank angle measurement is one of the most common solutions for production applications because of its reliability, durability and cost effectiveness. However, in practice, this system always produces considerable deviation from the actual crank angle position caused by mechanical and operating sources [4] [5]:

- The manufacturing tolerance of the flywheel and the number of teeth.
- Installation errors: eccentricity, swash, and sensor air gap variations.
- The relative displacement between the pickups and the shaft due to shaft bending, shaft longitudinal movement, and torsional vibration.
- Inductive sensor vibration caused by the engine block vibration because of the component coupling.
- Other sources of error: electromagnetic interference and time delay.

Except for the above-mentioned main sources of error, pressure pegging and TDC offset determination also contribute to errors in a pressure-based analysis [6]. However, these have been discussed in many research works, therefore they are not considered in this paper. For this work, the pressure and crank angle measurement sources of error are summarized and magnified for marine and power plant production applications in order to provide a starting step for error reduction and system accuracy improvement. Additionally, the error effects on IMEP and CA50 are also derived to obtain a connection with the engine control accuracy requirements.

Analysis of System Configuration and Datasets

In this paper, all the data that have been used are mainly from four different sources:

- Cylinder pressure data is obtained from a 10-cylinder Wärtsilä 31 gas engine. This pressure data in measured at 0.1 CAD resolution in compression and combustion strokes, while in inlet and exhaust strokes 1 CAD resolution is applied. Therefore, the compression and exhaust strokes' pressure data are linearly interpolated into 0.1 CAD resolution. Then the interpolated pressure data is used to do all combustion-related parameter calculations, such as IMEP, CA50, and THR. Furthermore, the measurements error impacts induced by thermal shock, swash, eccentricity and torsion are also quantified through these pressure data.
- The calibration data are processed to provide a general accuracy result of the pressure transducers that are used in production engines.
- Wärtsilä Finite Element Method (FEM) simulation results from different engines are used to quantify the crankshaft torsion and longitudinal movement, flywheel centre movement and tilting, engine block movement, and cylinder volume deformation.
- The cylinder pressure transducer manufacture's configuration data is used to estimate the overall accuracy of the cylinder pressure measurement system.
- Wärtsilä testing results are used to present the phenomena of cylinder pressure transducer thermal shock and the effect by installation.

Moreover, the cylinder configuration and crank angle measurement setup are showed in Figure *1*:

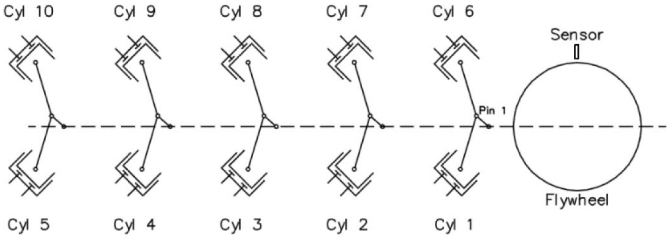

Figure 1. Measurement setups in this work

The IMEP, heat release rate (HRR), cumulative heat release (CHR) and CA50 are calculated on the basis of formulas 1 to 4:

$$IMEP = \frac{1}{2 * Vs} \sum_{i=i1}^{i2} P(i)(\mathrm{V(i+1)} - \mathrm{V(i-1)}) \tag{1}$$

$$HRR = \frac{K}{2 * (K-1)} P(i)\big(\mathrm{V(i+1)} - \mathrm{V(i-1)}\big) + \frac{1}{2 * (K-1)} V(i)\big(\mathrm{P(i+1)} - \mathrm{P(i-1)}\big) \tag{2}$$

$$CHR(i) = \frac{1}{2} \sum_{i3}^{i4} (HRR(\mathrm{i+1}) + HRR(i-1)\,) \tag{3}$$

$$CA50 = CAD(0.5 * \max(CHR)) \tag{4}$$

Where $P(i)$, $V(i)$ and $HRR(i)$are the cylinder pressure, cylinder volume, and heat release rate at crank angle degree i respectively. Vs is the cylinder swept volume, while CAD means the crank angle of the computed value. K is the specific heat ratio. $i1$ and $i3$ are the crank angle positions at the beginning of the meaningful calculation cycle; $i2$ and $i4$ are the crank angle positions at the end of the meaningful calculation cycle.

The objective of this work is to derive general conclusions about the cylinder pressure and crank angle measurement accuracy which are utilized for typical marine and power plant production engine control.

Cylinder Pressure Measurement and Error Analysis

Based on the piezoelectric phenomenon, piezoelectric pressure transducers are commonly used in production engines condition monitoring and fault diagnosis. From Figure *2* it is clear that, for this work, ±1 bar pressure offset leads to around ±0.6% of CHR error; and Table *1* shows that with ±1 bar pressure offset, the CA50 has a

maximum ±1.5 CAD error when 0.1 CAD measurement and calculation resolution is applied. Those are significant for combustion analysis and control. Therefore, for advanced engine control, to evaluate the sources of error and try to reduce the error is demanded for high accurate pressure data.

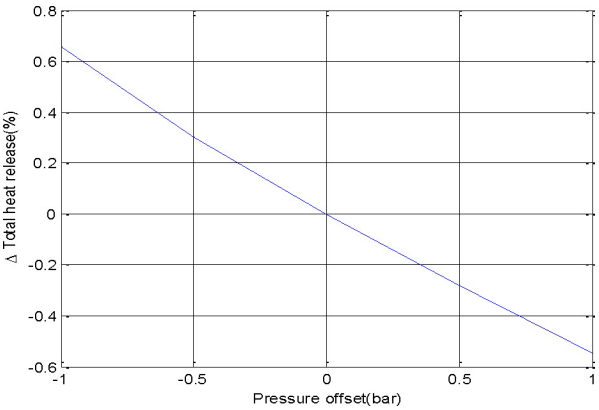

Figure 2. Total heat release with pressure offset

Table 1. Cylinder pressure measurement error impacts to combustion indicators

	CA50 Range (CAD)	Total CHR
Pressure ±0.1 bar	± [0 0.4]	± -0.06%
Pressure ± 0.5 bar	± [0.4 0.9]	± -0.3%
Pressure ± 1 bar	± [0.9 1.5]	± -0.6%

Sources of Pressure Measurement Error

Production piezoelectric pressure sensor consists of a pressure transducer and a charge amplifier. The pressure transducer responds to pressure variations, and a charge referenced to an arbitrary ground is generated and converted to voltage in the charge amplifier. Subsequently, the measured pressure value is referenced or pegged to a known pressure value. During the whole measuring process, because of the transducer property, demanding operating environment, and installation specification, the measurement accuracy is limited.

Thermal Shock

Due to the extreme operating environment, a transducer will suffer from heat transfer effects, a so-called thermal shock. The thermal shock is caused by the high heat flux which can distort the pressure transducer diaphragm, changing the transducer sensitivity. It is a cyclic thermal drift. Literature exhibits that thermal shock occurs during the combustion stroke and will immediately start to dissipate and recover, thus the exhaust stroke is the best phase to analyze its presence and severity [7]. A thermal shock can be evaluated by many different methods: using a dedicated heating test rig to measure the response of the transducer to an external heat load, a comparison of the measured signal with a calculated or simulated pressure, by using a reference transducer which has a much higher resistance to thermal shocks in the same cylinder [8], pressure deviation [9], a quasi-steady-state test, applying the average cylinder pressure during exhaust stroke as a function of the combustion phase and comparison of signal envelopes [7].

To detect the presence of a thermal shock, the methods based on signal upper envelope (USE), signal lower envelope (LSE) and signal average envelope (ASE) and pressure deviation are applied in this work. With a 1 bar difference between the upper and lower signal envelopes, Figure *3* indicates a relatively high thermal shock when compared with the result from [7] which is used as a reference sensor with a 3kPa (0.03bar) difference in USE and LSE.

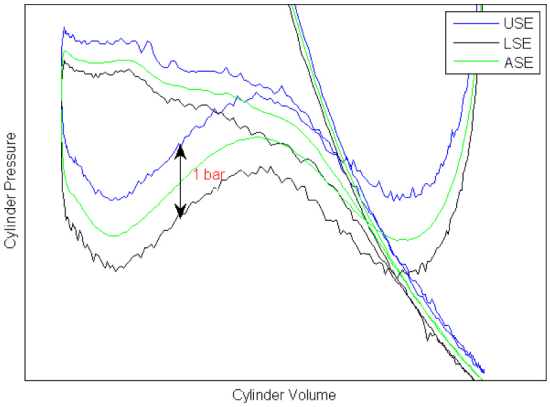

Figure 3. Thermal shock detection with signal envelope method

Another approach is based on the pressure deviation method which is applied in [9]. It is applied by comparing the cycle-to-cycle variance of the cylinder pressure at specified moments along the whole cycle. In theory, because of the random combustion process, the cycle to cycle variability is normal. Furthermore, this variability leads to changes in the pressure transducer thermal load, and when a thermal shock occurs, the sensitivity of the transducer will be changed and the scattering of pressure measurements will be enlarged. Thus the pressure variance scattering is used to indicate the presence of a thermal shock. As shown in Figure *4* where during 100% load operation, the water-cooled and uncooled sensors show obvious non-overlapping during the exhaust stroke. This non-overlapping continues until the late exhaust stroke. And in the late exhaust stroke, the pressure curves are overlapped again because of the dissipation of the thermal shock.

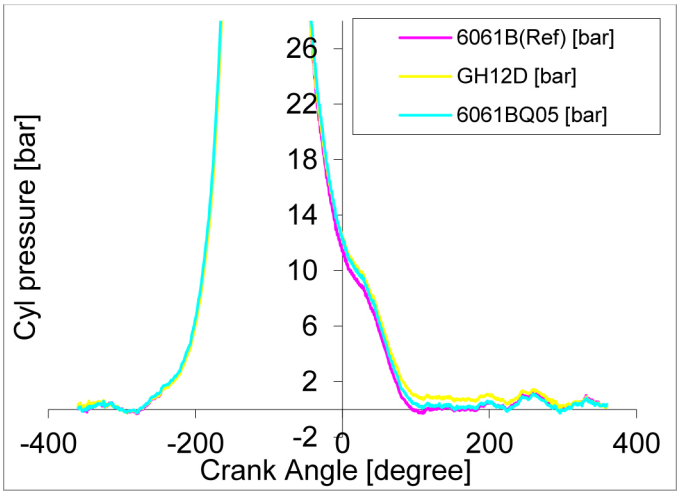

Figure 4. Water-cooled and uncooled pressure transducer comparison without TDC offset correction

Therefore, in this work, two points along the cycle are considered: the beginning of the exhaust stroke after the blow-down phase (238CAD after TDC) where the combustion variance influence is minimized, while the thermal shock effect still exists, and the compression stroke point (100CAD before TDC) which represents the cooled transducer. The pressure deviation from the mean value of 300 consecutive cycles are calculated to estimate the scattering of the pressure measurement:

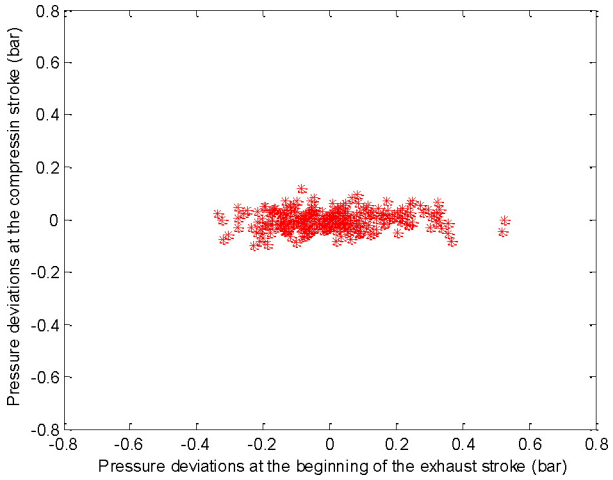

Figure 5. Thermal shock detection with pressure deviation method

As mentioned in [9], the pressure deviation in the exhaust point should have greater scattering than in the compression point. And Figure 5 reveals the same result, these result meaning that a thermal shock does exist in this test.

Although both methods indicate that a thermal shock does exist in this work, however, it is difficult to distinguish the effects of combustion variance, pegging, and the thermal shock. Therefore, a further test in a real engine by a comparative measurement with a reference sensor is planned for the future work to evaluate the methods used in this work.

A thermal shock is higher at low engine speed and at higher load, because of the longer cycle time and the higher cylinder pressure increasing rate. It is typically reduced by mechanical methods, such as coating the transducer diaphragm with silicon, the use of a transducer housing to compensate for thermal stress, recess mounting of the transducer, water-cooling, etc. An empirical equation based compensation method has also been researched in a numerical approach [10].

Installation

The sensor position and mounting method affect the reliability of the cylinder pressure signal and lifetime significantly. The choice of the mounting location should prioritize well-cooled regions of the head and avoid thermal stress. The diaphragm of the sensor should be positioned as recommended by the manufacturer. The sensor must be close to the flame plate level in the cylinder head flush mounted, since locating it below the flame plate will cause overheating. Furthermore, too high installation position in the bore can get a wrong peak signal because of pipe ringing which can easily destroy the sensor. Empty spaces between the membrane and cylinder head must be avoided particularly in gas engines because of the possibility that the sensor is destructed by the afterburning process. A central sensor location within the combustion chamber is recommended for knocking detection [11]. The optimum mounting is to flush mount the transducer into the combustion chamber, giving the highest bandwidth. In the case of flush mounting is not possible, the indicating bore should be short and with the largest possible diameter because of the acoustic oscillations.

A test which is carried out by Wärtsilä is used here to demonstrate the impact of the location on the cylinder pressure measurement accuracy. In this test, four cylinder pressure sensors of the same type are mounted in the same cylinder with evenly distributed locations, as showed in Figure 6. And the result is used to visualize the impacts from the location of the pressure measurement and knocking detection.

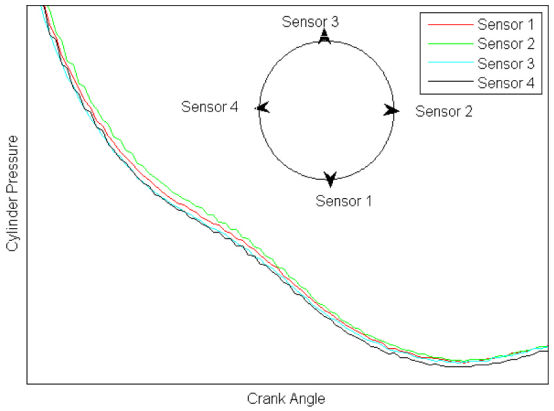

Figure 6. Pressure signal in different locations

Figure 6 shows that with this configuration, the maximum pressure difference at the exhaust phase is 1 bar. Therefore, for multi-cylinder engine, same location in all cylinders is better for cylinder balance control. Moreover, thermal shock effect is detected for different locations. Figure 7 shows that sensor 3 suffers from a relatively lower thermal shock, while sensor 2 and 4 have higher thermal shock.

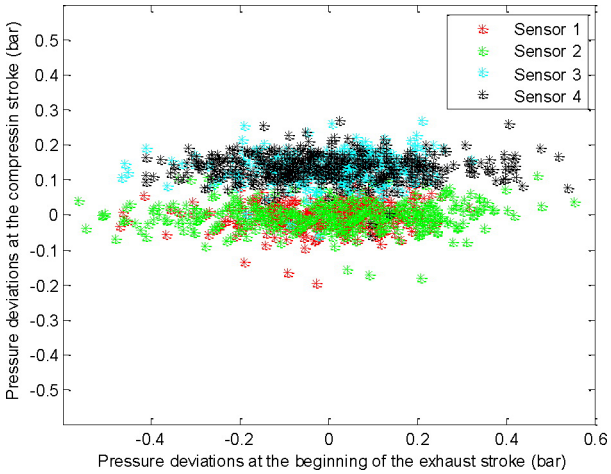

Figure 7. Cylinder pressure deviations for sensors in different locations

Cylinder Pressure Transducer Accuracy Calibration

Transducers must be calibrated against some standard in order to achieve a reliable result. Both static and dynamic calibration methods are commonly used for cylinder pressure transducer calibration. Dead Weight Tester (DWT) is a commonly used static calibrator. It works in the manner that a static test pressure is produced by manual adjustment

of the pump. Dynamic calibration is generally based on dynamic calibrators which can generate periodical (sine wave) or aperiodic pressure (single pulse, step and shock waves) waves for calibration.

Research shows that the time constant of piezoelectric transducers should be at least 10 times longer than the duration of the measured cyclic signal in order to eliminate the error due to attenuation of the signal within 1% (1). Regarding the piezoelectric transducers used in this work, the time constant is 10 to 30 seconds, which means that the output signal will decay towards zero before the event is completed. Thus DWT is not feasible for piezoelectric transducers. Therefore, in this work, two sets of calibration are applied in order to evaluate the performance of the transducers under variable temperature and pressure. DWT is used to calibrate the five piezo resistive pressure transducers, whereas, LEMAG TECHmag dynamic calibrator is used to calibrate five piezoelectric transducers.

The five piezo resistive pressure transducers are calibrated with DWT at the same time with three different temperature set points, 23.4 °C, 100°C and 200°C, in order to achieve a static and reliable result. Subsequent to calibration, the averaged pressure deviation under different calibration temperatures is calculated and shown in Figure *8*:

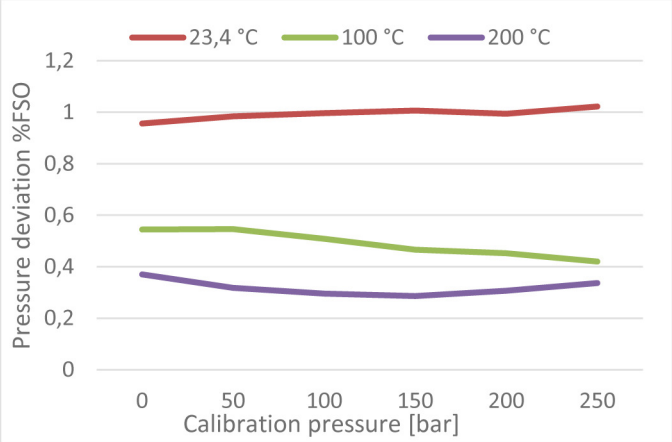

Figure 8. Pressure deviation for different calibration temperatures during static calibration of the piezo resistive transducers

Figure *8* shows clearly that calibration under ambient temperature has the lowest accuracy, while at 200 °C the result is the best. The averaged pressure deviation in 200°C is less than 0.4%FSO (Full Scale Output) which is much less than 1%. This is the consequence of the nominal calibration temperature of those five piezo resistive transducers is 200°C. Therefore, calibrating under right temperature is highly recommended in order to achieve a reliable result. Moreover, this result is only static calibration and thus only a sensitivity change since temperature and linearity are included.

LEMAG TECHmag calibrator is used to generate a dynamic pressure pulse, and a calibrated Kistler 6013 piezo resistive sensor is used as a reference sensor. Five piezoelectric test sensors are calibrated against this reference sensor. This dynamic calibration is done at room temperature, thus the thermal impact is not included. The whole calibration system set-up is shown in Figure 9 where the reference and test transducers are installed on the calibrator, the output from the reference transducer is connected to a charge amplifier, the test sensor signal output is converted into voltage by a 4mA=1V=0bar and 20mA=5V=300bar converter, and both signals are transmitted to DEWEsoft I/O and finally to a DEWEsoft user interface. In the DEWEsoft interface, the pressure data of a few cycles are acquired after 6 minutes of running. The reason for doing it in this way is to stabilize the pressure data and achieve reliable calibration results. The pressure data is obtained by considering 4 consecutive cycles for each test sensor and comparing the result with the reference sensor.

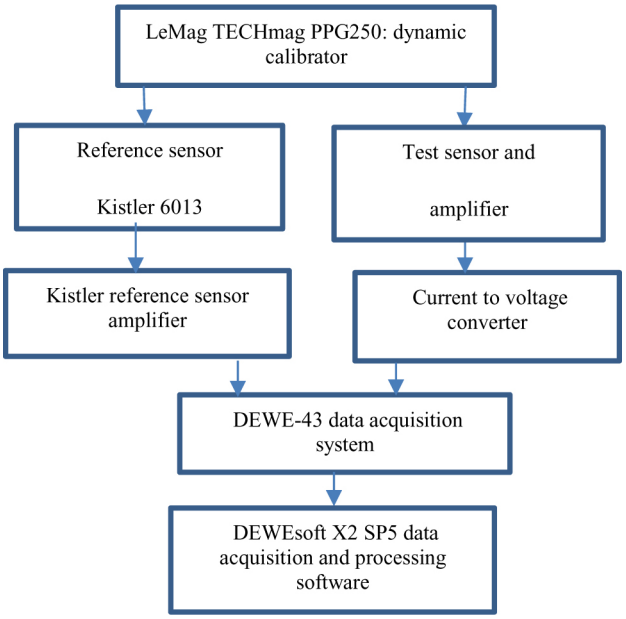

Figure 9. Structure of the dynamic calibrating system

The one point that needs to be highlighted is the time constant of the charge amplifier. Concerning the transducers that are used in this work, the time constant is between 10 to 30 seconds, thus during calibration the reference transducer should also use the same or a similar time constant value. That being so the pegged pressure curves will not have obvious disengagement after pegging window. In this work, a medium time constant is used for the reference pressure sensors charge amplifier.

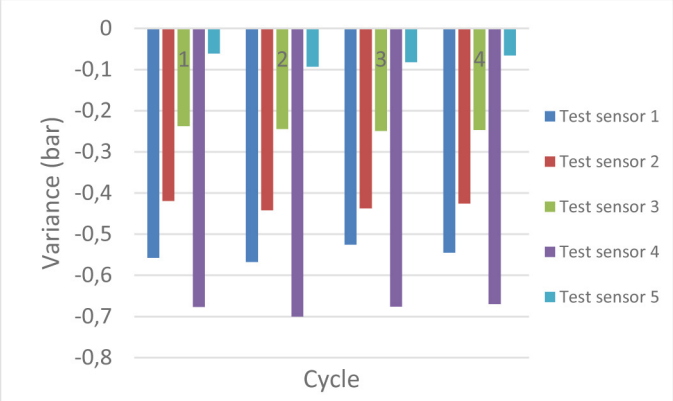

Figure 10. Peak pressure amplitude variance during dynamic calibration of the piezoelectric transducers

In order to evaluate the test transducer performance, the peak pressure (PP) and its location (LPP) are compared with the reference transducer. For PP evaluation, a short windowing pegging method is used to adjust the offset level by comparing the difference between the reference and test pressure data. The mean within this window is defined as the test sensor pressure offset. However, because of the pegging windowing selection, the PP amplitudes may change according to the reference

sensor baseline. Therefore, this peak pressure value evaluation can only be regarded as a relative result. The LPP is obtained through a two degree of polynomial fitting process. The following Figure *10* shows the result of the peak pressure variance:

Figure *10* exhibits that the peak pressure amplitude variance is up to 0.8 bar below zero when the maximum calibration pressure 140 bar is reached. The peak pressure stability experiences -0.4bar mean difference and 0.22 standard deviation. The test sensor in general gives a lower peak pressure than the reference sensor with this windowing pegging method. Regarding LPP, after data fitting the variance is 0.

The test pressure sensor offset is monitored to quantify the baseline stability. It is done by comparing the pressure offset variance separately. Figure *11* shows the pressure variance compared with its own previous cycle.

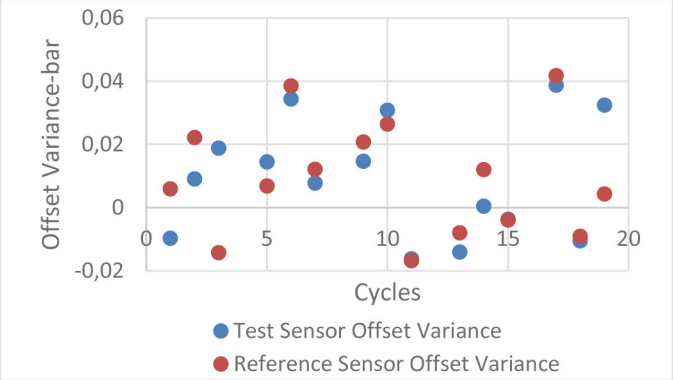

Figure 11. Offset variance when compared with previous cycle during dynamic calibration of the piezoelectric transducers

Figure *11* indicates that the pressure offset for the test sensor and the reference sensor have a similar scattered distribution and amplitude. The cycle-wise offset variance is within ±0.05 bar. Both the test sensor and the reference sensor have a mean offset variance of 0.01 bar with a 0.02 standard deviation. Therefore, the test sensor performs similarly to the reference sensor.

It is obvious that the peak pressure has a significant impact on the pressure offset values. Within the similar peak pressure range, the offset is relatively stable. This also proves that the main drawback of a piezoelectric pressure sensor is the instability of the baseline.

This calibration result gives a general conclusion that, without the thermal effect, the performance of the test sensors compared to the reference sensor are very similar. Table *2* summarized the calibration result of the compared parameters:

Table 2. Dynamic calibration result of the five test sensors compared to a reference sensor

	Mean Variance	STD
Peak Pressure Amplitude	-0.4 bar	0.22
Location of Peak Pressure	0	0
Test Sensor Pegging Variance	0.01 bar	0.02
Reference Sensor Pegging Variance	0.01 bar	0.02

The results shows that the test sensor has similar performance with the reference sensor. However, in practice, the thermal effect is one of the main challenges which affects the sensor accuracy. In order to estimate the accuracy of the pressure measurement chain looking into every step in the measurement chain and combining the tolerances for all equipment and processes would be beneficial. The main error sources of pressure measurement are the pressure transducer and the signal input/output transmission and processing. Additionally, their accuracy is estimated on the basis of the manufacture's configuration data in Table *3*.

Table 3. Cylinder pressure measurement chain datasheet

Cylinder pressure sensor accuracy	±1.2%
Signal processing module accuracy	±1%

To sum up the results, a guide which provides general rules considering evaluating and expressing uncertainty in measurements (GUM), is used [12] [13] . In this work, all the uncertainty calculations are based on method B and the error distribution functions have a rectangular distribution because of the error characteristics. The uncertainty listed is the expanded uncertainty based on different coverage factors calculated in accordance with the GUM. For this work, 250 bar measurement range is considered, and the total pressure measurement uncertainty is showed in Table 4:

Table 4. Cylinder pressure measurement chain accuracy

Uncertainty Source	Standard Uncertainty Calculation (%)	Standard Uncertainty (%)	Distribution
Cylinder pressure sensor	1.2	6.93E-01	Rectangular
Signal processing module	1	5.77E-01	Rectangular
	Combined Standard Uncertainty	0.90	
Level of Confidence	Converge Factor	Expanded Uncertainty (%)	Expanded Uncertainty (bar)
68.27%	1	0.90	2.25
95.45%	2	1.80	4.51
99.73%	3	2.71	6.76

The correct approach in reading Table 4 is: approximately 68.27% of the obtained cylinder pressure signal in a control unit has the uncertainty of ±2.25 bar, and 99.73% of the obtained cylinder pressure signal in a control unit has the uncertainty of ±6.76 bar. As Figure *2* exhibits even a 1 bar error can lead to a significant error in combustion indicators. Therefore, the error uncertainty here in the whole measurement chain is significant for the closed-loop cylinder-pressure-based combustion control. Here in fact, a novel thermodynamic-based pegging method is used, so less sources of error are included when compared with a traditional inlet-pressurebased method.

Crankshaft Position Measurement and Error Analysis

Regarding the thermodynamic analysis, pressure data needs to be processed in an angular domain. Corresponding to each measured cylinder pressure value, its actual crank angle is extremely important since a variety of parameters are derived from it: the IMEP, HRR, CHR, CA50, combustion duration etc. A small error in the cylinder pressure phasing can lead to a serious error in the calculation of the thermodynamic parameters. As shown in Figure *12*, a ±1 crank angle degree error leads to around ±1.8 bar IMEP error. IMEP is one of the most critical parameters for engine balancing and combustion control, and therefore, high accuracy crank angle measurement and phasing are undoubtedly required.

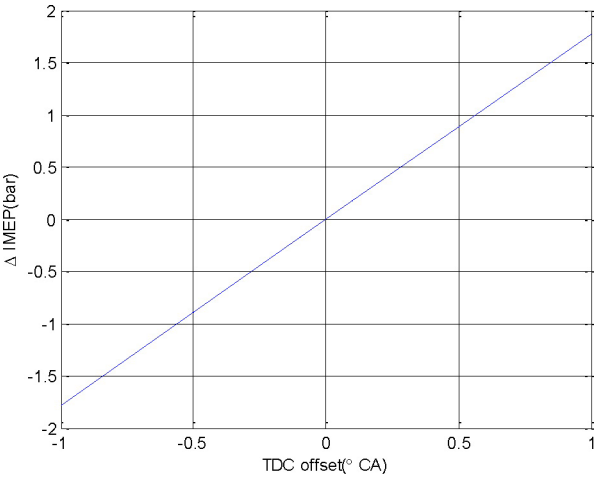

Figure 12. Influence of crank angle error on IMEP

Moreover, Table *5* lists the impacts from the crank angle measurement error on some typical combustion indicators which include IMEP, CA50, and THR.

Table 5. Crank angle measurement error impacts on combustion indicators

	IMEP (bar)	CA50 Range (CAD)	THR
Pressure TDC offset ± 0.1 CAD	±0.18	±[-0.1 0]	±0.35%
Pressure TDC offset ± 0.5 CAD	±0.89	±[-0.4 0]	±1.75%
Pressure TDC offset ± 1 CAD	±1.77	±[-0.6 -0.1]	±3.5%

Table *5* recommends that in this work, in order to achieve a ±0.9 bar deviation for IMEP, the requirement for TDC offset is ±0.5 CAD. Furthermore, the THR gets an error of around ±3.5% from a ±1 CAD crank angle measurement error. Accordingly, the crank angle measurement uncertainty is within ±0.5 CAD, and therefore, the THR error is around ±1.75%. Moreover, the deviation of CA50 is within ±0.6 CAD when 0.1 CAD measurement and calculation resolution is used in this particular case.

In practice, there are two different methods for angular position measurement: a crank angle encoder and toothed/slotted wheel-based pickups. According to literature, a crank angle encoder is considered to have a higher accuracy, and an encoder can also be used to trigger the measurement of a pressure signal, which will lead to a better phasing. However, it is challenging to use an encoder in production engines because of the installation modification, cost, and reliability, especially for large marine and power plant engines. Thus, in industry, usually a toothed/slotted wheel with an inductive sensor is used to measure the crank angle in production engines. With this configuration, in the following part, all the sources of error are analyzed and quantified on the basis of simulation and theory calculations from four-stroke large bore marine and power plant engines. Furthermore, their impacts to IMEP and CA50 are also calculated because of their importance for engine control.

Sources of Error

An inductive sensor consists of a permanent magnet with a ferromagnetic core surrounded by a coil, as shown in Figure *13*. It is usually mounted with an air gap d to the ferromagnetic teethed or slotted flywheel. When teeth or slots pass through the sensor's magnetic source, which means the crank angle position φ changes, the magnetic flow $\varnothing M$ is changed, and an electric analog signal is generated.

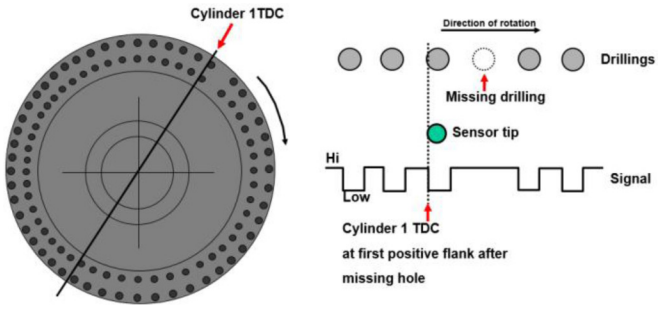

Figure 13. Crank angle measurement signal generation

The frequency and amplitude of this analog signal are proportional to the rotating velocity. This induced analog signal V can be calculated as:

$$V = W * \frac{\partial \varnothing M}{\partial \varphi} \frac{\partial \varphi}{\partial t} \tag{5}$$

Here $\varnothing M = \varnothing M(\varphi, d)$ and W is the windings of the coil. The formula also indicates the main factors which have an effect on the output voltage signal, the coil design, the flywheel consecutive angle, the air gap, and the time or engine speed. Thus any factors that can impact any of the above will influence the accuracy of the crank angle measurement. Moreover, this voltage signal will be converted into an ON/OFF signal by the engine control unit (ECU) through the rising edge or falling edge. With this signal, one missing slot is used to identify the top dead center (TDC) for one specific cylinder which is defined as the slot after the missing slot.

Regarding advanced combustion monitoring and control, demands on accurate engine speed and angular position measurements are increasingly important. Previous work demonstrated that, the angular variations in the magnitude of 0.05 degree have a significant impact on the measured engine speed and angular position and must therefore be compensated [14]. Consequently, nowadays the hall sensor is also commonly used because of the direct generation of the ON/OFF signal and its reliable performance.

Manufacturing Tolerance of Flywheel Slots

Manufacturing tolerance of the flywheel slots, implies that it is impossible to get evenly distributed slots or teeth on the flywheel, and therefore, the deviations of the actual angles from the ideal values will introduce a geometrical error to the measurement. Research showed that, for misfire detection, the slot angle errors in the magnitude of 0.06 degree can increase a number of misclassifications from 0.01% to more than 6% [14]. Moreover, this error source also has a negative impact on the crankshaft angular velocity measurement, thus this error must be considered and compensated.

In this work, a flywheel configuration with 120 circle slots is considered. Among them 119 slots are marked on the wheel and 1 slot is missing. With the structure as shown in Figure *14* where the distance from the center of the flywheel to the slot is 512.5mm, the radius of the slot is 7mm with the defined maximum position tolerance of 0.2mm.

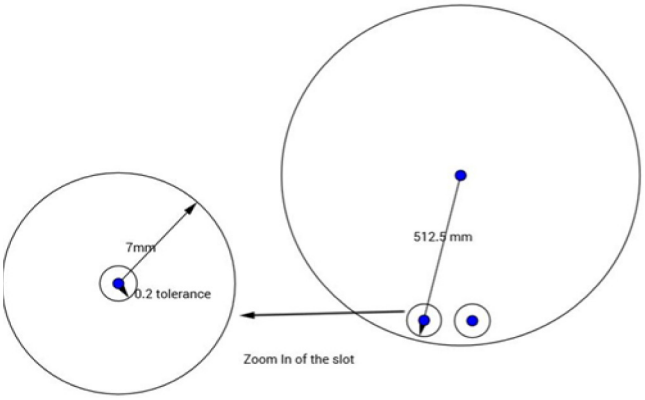

Figure 14. Flywheel and slots structures

Considering this maximum 0.2 mm tolerance, it is the same as the center of the slot also having a 0.2 mm tolerance. Consequently, the tolerance in angular domain ∅ can be calculated.

$$\sin\emptyset = \frac{0.2}{512.5 - 7} \tag{6}$$

As a result, ∅ is around 0.023 degree, and the maximum tolerance is equal to two consecutive slots having the same direction tolerance which means a 0.023*2= 0.046 degree error. Although this error is smaller than 0.06 degree which is defined as the value of increasing the amount of mis-classifications of misfire, a further evaluation is applied to evaluate the impact of this error by considering the worst case, and subsequently, the error is generated when the consecutive slots (3 CAD) have opposite direction error of ±0.046 CAD error. Eventually with 0.1CAD resolution, this error is divided equally and added to all the measured crank angle data. Afterwards in the calculation it is concluded that the IMEP has an absolute mean error of $4.43*10^{-5}$%. Regarding heat release analysis, CA50 is also calculated. On the basis of the error direction, with the unequally distributed slots on the flywheel, the CA50 has a [0 0.1] CAD error, when crank angle measurement resolution is 0.1 CAD.

This manufacturing error can be compensated by additional signal processing, such as the method based on energy balance equation, while the adaptive method based on the chi-square test is also used to compensate the unequally distributed slots via a variable reluctance sensor [15] and additional sensor expanding method [16].

Moreover, the slot or tooth number on the flywheel defines the angle interval which impacts the crank angle measurement resolution and accuracy significantly. Increasing the slot number on the flywheel or interpolation can be used to increase the resolution of the crank angle measurement.

Installation Error

In addition to the manufacturing imperfection, the installation of the flywheel and inductive sensor will introduce errors, such as flywheel eccentricity, swash and the sensing gap changing as well. In practice, by comparing with the first cylinder TDC position, the flywheel is adjusted in order to indicate the first cylinder TDC correctly. This manual process cannot guarantee a perfect result, and is therefore prone to error. Moreover, the sensor installation position and its stability have a strong impact on the output signal. Although the position error can be corrected in the control system, unreliable installation or abnormal operation may generate vibration, and this can introduce significant errors on the sensor output signal.

Eccentricity or run-out means that the wheel is not rotating around its geometric center but, instead, the center has a displacement. It is showed in Figure *15* where *O* is the geometric center and *O'* is the rotating center. *Θ* is the measured crank angle and *Θ'* is the rotating angle. It is at the first engine order.

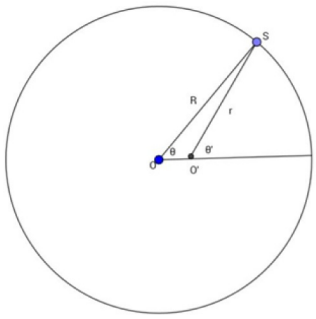

Figure 15. Eccentricity error

Research work showed that even a small eccentricity error, can lead to significant errors in the measurement of the engine speed and angular position [4].

Figure *16* is the FEM simulation result from Wärtsilä AVL Excite of the flywheel center movement. It shows that the flywheel center moves more frequently to the upwards direction. This is easy to understand when the ignition time is earlier than TDC, thus the force going upwards is greater than the one going downwards. In the following, a formula from work [4] is used to calculate the measured angle error considering the eccentricity error:

$$\Delta\phi = \frac{oo'}{R} * (\sin(\theta + \Delta\theta) - sin\theta) \tag{7}$$

oo', the maximum central displacement can be considered. $\Delta\theta$ is the flywheel slot difference, here it is 3 degrees when the flywheel has 119+1 slots. R for this simulation is 635.5mm. The eccentricity error is shown in Figure *17*. This error is in a positive direction with the crank angle measurement, which means that the real crank angle is the sum of the measured value and the error. Using multiple read heads can reduce the eccentricity error. The maximum eccentricity error is around 0.04mdeg. Based on the eccentricity error, the crank angle can be corrected and the volume can be calculated accordingly. By comparing with the un-corrected crank angle, the IMEP difference is of absolute mean 1.46*10^ (-4) %, and CA50 has a zero difference. Using multiple read heads can reduce the eccentricity error.

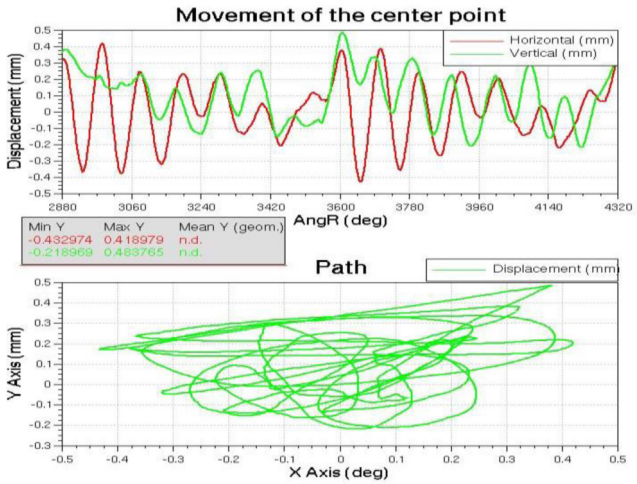

Figure 16. Movement and path of the flywheel center point

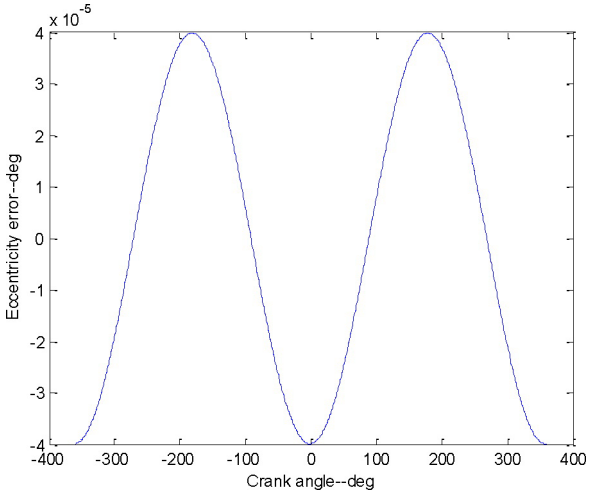

Figure 17. Eccentricity error result

Swash indicates the geometric axis inclination to the rotating axis; which will cause a geometric slot pitch tolerance. Both eccentricity and swash can change the distance between the mark and the pickup sensor, in addition to introducing errors to the output signal. To quantify the swash error, the overall tilting of the flywheel is explored within Wärtsilä by FEM simulation. Figure *18* shows the tilting error:

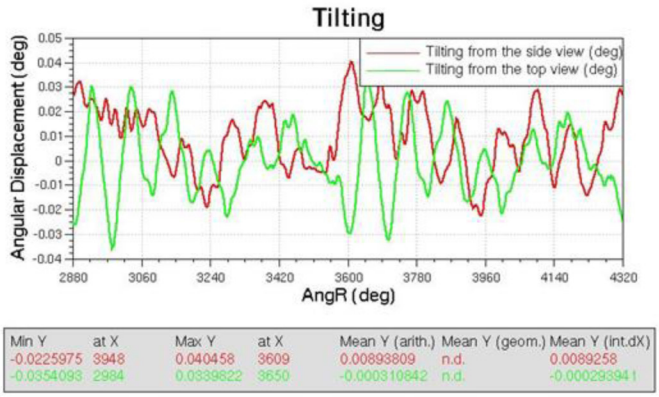

Figure 18. Flywheel tilting error

The formula [4] below shows how to calculate the swash error:

$$\Delta\phi = \frac{\varepsilon * w}{R}(\cos(\theta + \Delta\theta) - cos\theta) \tag{8}$$

Here R is 635.5mm, ε is the angle between the plane normal vector and the angular velocity vector which is the tilting angle from the side view from the simulation result. Thus ε has a maximum of 0.034deg displacement. w is the variation of flywheel slots or marks width. Subsequent to the calculation, the swash error is shown in Figure *19*:

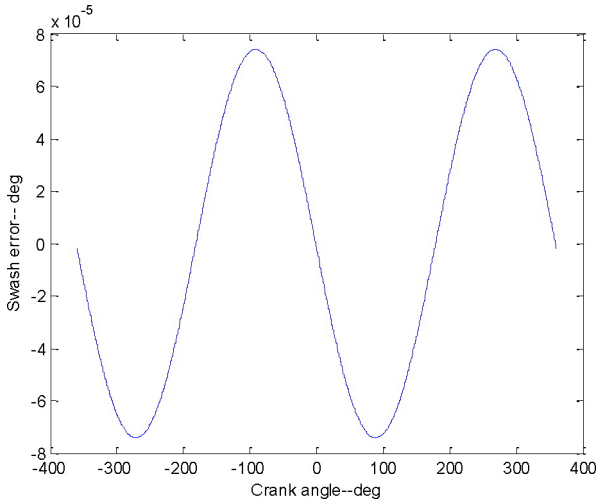

Figure 19. Swash error result

This error is in a negative direction with the crank angle measurement, which means that the real crank angle is the subtraction of the measured value and the error. The maximum swash error is around 0.074mdeg. On the basis of the swash error, the crank angle is corrected and the volume is calculated accordingly. By comparing with the un-corrected crank angle, the IMEP difference has an absolute mean of 1.3*10^ (-4), while CA50 has a zero difference. Respectively, in this work, the eccentricity error and swash error are similar and both have relatively small effect on the volume and IMEP calculations. The unequally distributed slots, eccentricity, and swash errors can be compensated through signal processing and previous deviation parameter identification [5].

Furthermore, the air gap between the crankshaft pick-up and the flywheel should be within the nominal limit. During installation, this air gap accuracy is limited by the micrometer that is used to verify the critical dimension. With the new generation of sensors, the air gap can be controlled more accurately since a more flexible air gap is provided, meaning that the output signal will not be dependent on the air gap as much as before, and therefore a larger air gap is allowed.

Relative Displacement between the Pick-Ups and Shaft

It is known that, because of the mechanical connection, gas forces, mass and fluctuating torques are generated at the crankshaft. Thus vibrations are imposed on the crankshaft and the TDC of each cylinder may deviate from the reference value. Because of the torsional vibrations, shaft longitudinal movement and shaft bending, there will be a relative displacement between the pick-ups and the shaft. Figure *20* exhibits the geometry of the crankshaft and its three dimensional movements.

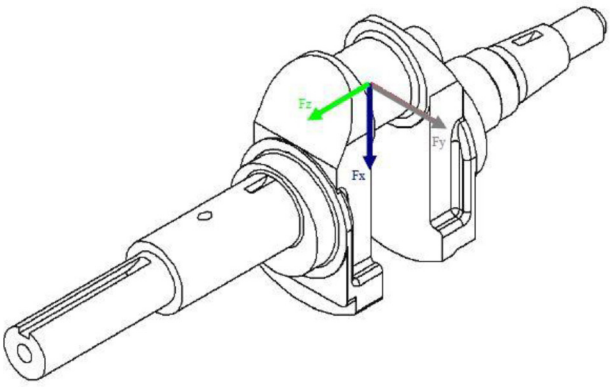

Figure 20. Crankshaft longitudinal displacement (Fz), bending (Fx) and torsional vibration (Fy)*[17]*

Especially with long or flexible crankshafts, the maximum torsion can be 1.5°CA at full load, and this may cause deviations of a magnitude of around 30% in the friction mean effective pressure (FMEP) and around 2% in the energy balance [18].

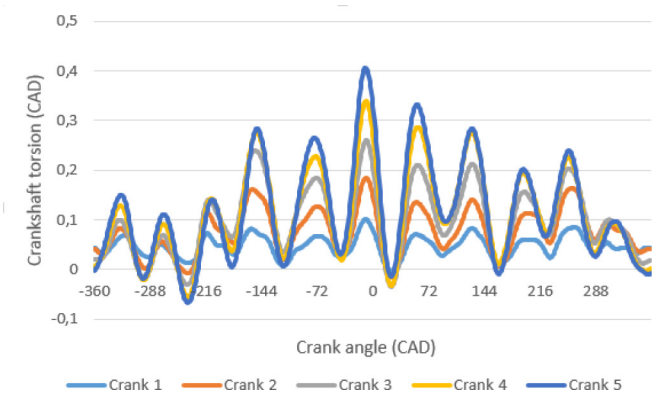

Figure 21. Simulated angle of torsional vibration of individual crankpins relative to flywheel

The effect of torsional vibration is more significant at certain engine speeds because of the resonance frequencies of the crankshaft. The torsion value can be validated by measuring the total torsion of the crankshaft between the flywheel and its front end. For a crank angle measurement system uncertainty analysis, the FEM simulation result from Wärtsilä is used.

FEM simulation with full load is used here to quantify the torsional vibration. This FEM simulation result includes the effects of torsional vibration and constant torque, and thus it is a transient simulation. The torsional vibration of every individual crankpin relative to the flywheel is shown in Figure *21*:

Figure *21* implies that the greater the distance from the flywheel of the engine, the greater the simulated torsion offset. Prior to the combustion phase, the torsional vibration for all cylinders is relatively small. The maximum vibration is around 0.41CAD. This error is in a positive direction with the crank angle measurement, which means that the real crank angle is the sum of the measured value and the error.

On the basis of the torsion curves from the crankshaft simulation, the measured crank angle can be corrected, and thus the volume can be corrected. Figure *22* illustrates the measured raw crank-angle-based PV diagram and the corrected crank-angle-based Pressure-Volume (PV) diagram for cylinder 5. Here the difference is amplified by 10 times.

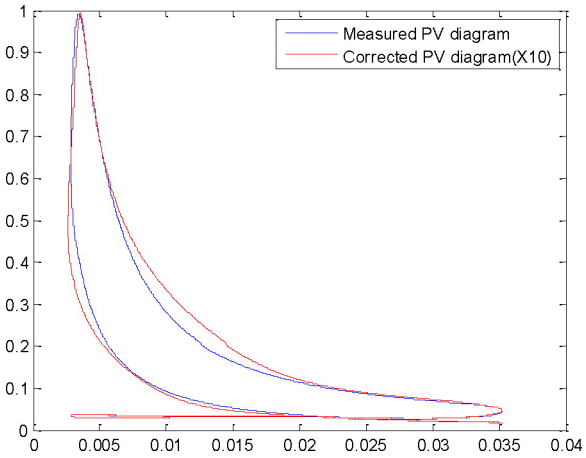

Figure 22. Measured and corrected PV diagram

The corrected PV diagram indicates a higher work output. And Figure *23* shows the volume difference after correcting the crank angle according to the simulation result. Here the difference is amplified by 20 times.

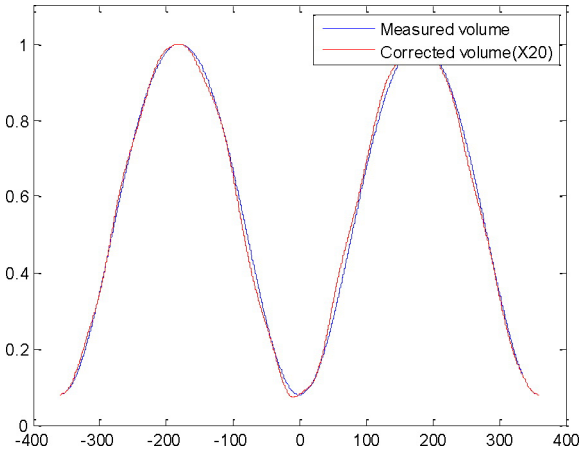

Figure 23. Measured and corrected volume

The volume difference is of absolute mean 0.17%. The influence of the crankshaft torsion on IMEP is showed in Figure *24* where the relative IMEP to a pre-defined reference level is calculated for all cylinders.

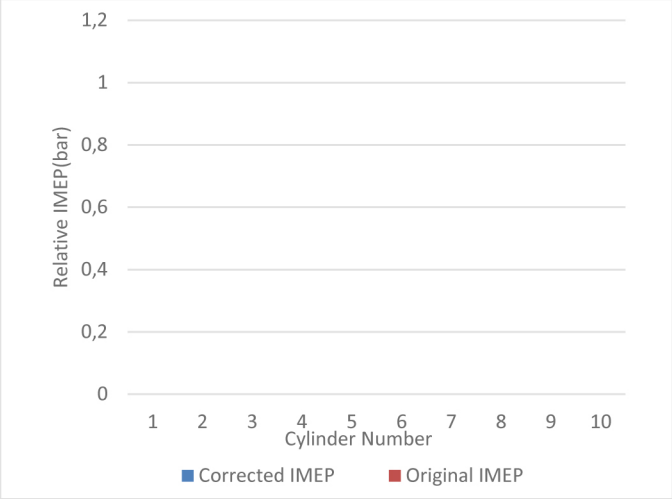

Figure 24. Measured and corrected IMEP

The comparison illustrates that with the corrected crank angle measurement data, the IMEP has a higher value. For each cylinder, the IMEP differences are listed in Table *6*:

Table 6. Measured and corrected IMEP difference

Cylinder number	1/6	2/7	3/8	4/9	5/10
IMEP difference	0.21% 0.22%	0.36% 0.38%	0.52% 0.52%	0.68% 0.7%	0.84% 0.85%
CA50	[-0.1 0]	[-0.1 0]	[-0.2 0]	[-0.2 0]	[-0.3 0]

Additionally, the CA50 difference is all within [-0.3 0] CAD because the calculation resolution used in this work is 0.1 CAD. And the further the cylinder is away from the flywheel, the more the IMEP and CA50 are influenced by the torsion. Thus this error has an effect on cylinder pressure diagnostics, especially for an engine with a long crankshaft with many cylinders.

Moreover, the axial or longitudinal movement of the shaft can change the air gap between the crankshaft pick-up and the flywheel slot easily. The gap distance will change the induced voltage and the output signal amplitude: the bigger the gap the smaller the signal amplitude, and the smaller the gap the bigger the signal amplitude. Figure *25* shows the FEM simulation and measured results of the maximum longitudinal movement of the crankshaft.

Figure *25* shows that the maximum displacement of the crankshaft is around 30% of the nominal air gap which is around 1-3.24mm, and thus attention is needed during installation. And for the new generation of measurement sensor which has much higher tolerance to the air gap, this displacement will not any more contribute to such significant error as a traditional sensor, and therefore a higher accuracy can be reached as well.

The motion of a crankshaft under the fluctuating forces applied by a connecting rod to a crankpin cause bending vibrations of the crankshaft. By simulation the maximum shaft bending both downward and upward is around 30% of the manufacturing tolerance. Therefore, this is negligible for the crank angle measurement system.

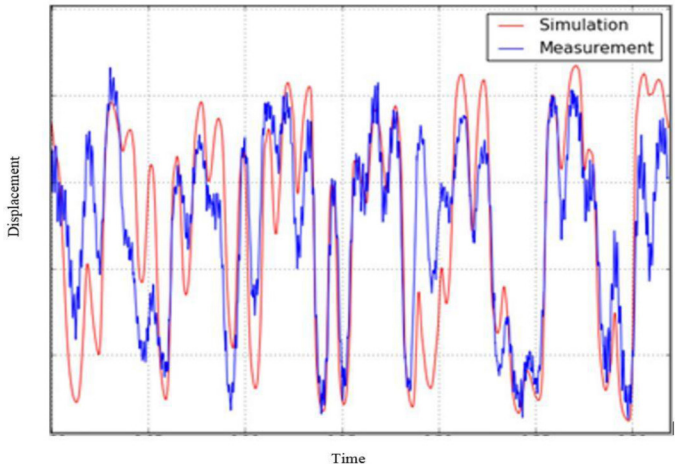

Figure 25. Longitudinal movement of the crankshaft

Inductive Sensor Vibration

Another possible error comes from the relative movement of the flywheel and the pick-up sensor because of the engine block movement. During operation, the engine block will vibrate and induce the inductive sensor to vibrate because of the mounting coupling. When vibration occurs, a pulse delay may happen because of the facing movement and fluctuant engine speed. Figure *26* shows the Wärtsilä FEM simulation result for the engine block vibration in transversal, vertical and longitudinal directions.

Considering the maximum vibration moment, meaning in this case that the engine speed is within the range of 850rpm to 860rpm. In fact, this is an extreme operating case because the speed range is already out of the nominal operating conditions. The time interval between two consecutive slots can be calculated accordingly:

$$\frac{60s}{855rpm * 120slots} = 0.0005848s/slot \tag{9}$$

Then the corresponding facing movement distance can be calculated based on velocity root mean square (RMS) amplitude *N* which can be obtained from Figure *26*:

$$0.0005848s * \frac{60mm}{s} = 0.035mm \tag{10}$$

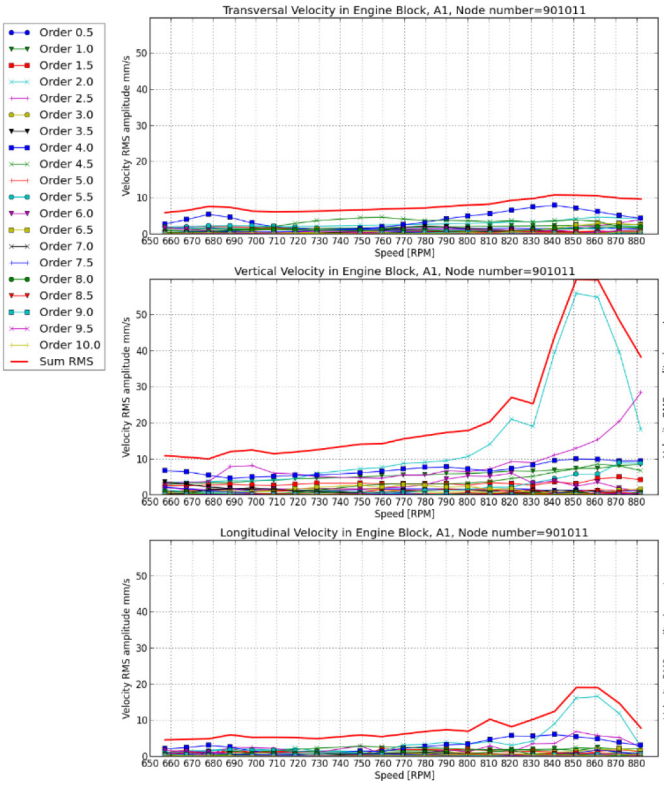

Figure 26. Engine block movement in different directions

Subsequently, the result here is an extremely small value even compared with the flywheel slots manufacturing tolerance of 0.2mm. Therefore, this source of error is negligible when compared with all the other above mentioned errors.

Other Sources of Error

Electromagnetic interference from magnetic pick-ups can also impact the output signal. Therefore, the mounting material should be non-magnetic to avoid signal interference and the air gap distance must be evaluated carefully.

In practice, the sensor should not be attached on a too soft mounting, which will in turn generate a displacement between the pick-up and the shaft or maybe even generate a fictive torsional vibration. Moreover, during calculation, the computation formula and the rounding error will also impact the extracted result.

Time delay which indicates the rising, falling edge delay and hardware delay, is also a potential source of error if high precise measurements are required, especially for high speed measurement. Meanwhile, for 120 holes flywheel, the crank angle needs to be converted into 360 degrees, which also introduces error. A test has been executed by Wärtsilä to test this delay, and the result shows that the maximum error that all those mentioned sources introduced is around 5mdeg when the speed is 1000 rpm. With this error, the absolute error of IMEP is around 0.03%. The CA50 difference is within [0 0.1] CAD. However, the time delay can be compensated because of the constant delay, and thus after compensation, the error can be much less than 5mdeg.

The pressure load, thermal expansion and bolt pretensions during the engine working cycle result in cylinder components deformation. The increase in the firing volume due to component deformations is calculated in this work. According to the Wärtsilä FEM simulation result, the volume is +2.4% higher than the nondeformed volume at 0 crank angle degree (TDC); and +3.2% higher than the nondeformed volume at 12 CAD after TDC (peak pressure location). In order to further estimate the deformation of the whole cycle, the volume deformation is assumed to have the same distribution as the mean pressure curve of 300 consecutive cycles. Therefore, the pressure curve is fitted with Matlab and scaled down to the deformation amplitude by using a smoothing spline function, as shown in Figure *27*:

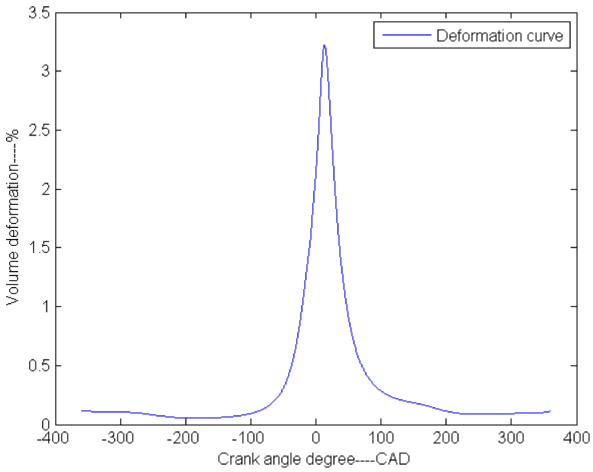

Figure 27. Estimated cylinder volume deformation curve

Table 7. Uncertainty of crank angle measurement

Uncertainty Source	Standard Uncertainty Calculation (%)	Standard Uncertainty (CAD)
Manufacturing Tolerance	0.046	0.027
Eccentricity	4.00E-05	2.309E-05
Swash	7.40E-05	4.272E-05
Torsion	0.24	0.139
Time Delay	0.0025	0.001
Volume Deformation	0.0395	0.023
	Combined Standard Uncertainty	0.143
Level of Confidence	Converge Factor	Expanded Uncertainty [CAD]
68.27%	1	0.14
95.45%	2	0.29
99.73%	3	0.43

As seen in Figure 27, after curve fitting, the amplitude of the curve is modified so that at 12CAD the deformation is 3.2%. Later the whole cycle deformation information is used to calculate the induced crank angle error, which yields a maximum error of ±0.079CAD. Furthermore, the induced impacts on other combustion parameters are also computed, while with this volume deformation, the absolute error of IMEP can be 0.78%. Regarding CA50, the difference is between [-0.9, -0.3] CAD. Therefore, cylinder volume deformation has a significant impact for combustion analysis.

Considering all the sources of error which are discussed in this work, a conclusion about the overall crank angle measurement system uncertainty (including cylinder volume deformation) is estimated on the basis of the GUM guide. While method B is applied on the basis of the error distribution characteristics. The overall uncertainty result is listed in Table 7.

From Table 7, the overall uncertainty of the crank angle measurement system in this work is approximately 68.27% of the measurements which have an uncertainty of ±0.14 CAD, and 99.73% of the measurements which have an uncertainty of ±0.43 CAD.

With all the sources of uncertainty for crank angle measurements, the worst-error cases are listed in Table 8, and their impacts on IMEP and CA50 (crank angle measurement resolution is 0.1 CAD) are also analyzed in order to outline their importance for combustion analysis.

Table 8. Crank angle measurement error span and impact on IMEP and CA50

	Maximum Crank Angle Error (CAD)	IMEP Error (%)	CA50 Error (CAD)
Manufacturing Tolerance	±0.046	$\pm 4.4*10^{-5}$%	[0 0.1]
Eccentricity	±0.04*10^(-3)	$1.46*10^{-4}$%	0
Swash	±0.074*10^(-3)	$1.3*10^{-4}$%	0
Time Delay	5*10^(-3)	0.03%	[0 0.1]
Torsional Vibration	0.41	0.85%	[-0.3 0]
Volume Deformation	±0.079	0.78%	[-0.9 -0.3]

Table 8 lists that for CA50, the uncertainty is [-1.2 -0.1] CAD. The volume deformation is an empirically estimated result. However, its significant impact on IMEP and CA50 must not be ignored. Thus the next step will be focusing on those two main sources of error and trying to eliminate their impact to a lower or even zero level.

To summarize the total uncertainty of IMEP, all the crank angle measurement sources of error which are discussed in this work are considered. In addition, according to the different error distributions the uncertainty of IMEP is calculated in % unit in Table 9:

Table 9. Uncertainty of the IMEP calculation result

Uncertainty Source	Standard Uncertainty Calculation (%)	Standard Uncertainty (%)
Manufacturing Tolerance	4.4E-05	2.54E-05
Eccentricity	7.30E-05	4.21E-05
Swash	6.50E-05	3.75E-05
Time Delay	0.015	8.66E-03
Torsion	0.425	2.45E-01
Volume Deformation	0.39	2.25E-01
	Combined Standard Uncertainty	0.33
Level of Confidence	Converge Factor	Expanded Uncertainty [%]
68.27%	1	0.33
95.45%	2	0.67
99.73%	3	1.00

Conclusion

In this work, the sources of error for a piezoelectric-based cylinder pressure measurement system and inductive-based crank angle measurement system are analyzed for typical marine and power plant production engines. Conclusions can be summarized as follows:

- The cyclic thermal shock is detected by signal envelope and cycle-to-cycle variance methods. In this work, the results of both methods indicate the presence of the thermal shock. The installation and location of the sensor has an impact on the amount of thermal shock.
- Regarding cylinder pressure sensor calibration, the calibration method selection and calibration temperature are important. It is recommended to calibrate the cylinder pressure sensors under nominal operating condition. Calibration in this work shows the importance of the calibration temperature and indicates that the test sensors in this work have small deviations with the reference sensor in the peak pressure, peak pressure location, and static pressure offset variance under room temperature.
- Considering the overall accuracy of the test sensor and the signal processing unit, the overall uncertainty of the obtained cylinder pressure signal for analysis and computation is finalized as follows: 68.27% of the pressure signals have an uncertainty of ±2.25 bar, and 99.73% of the pressure signals have an uncertainty of ±6.76 bar.
- With respect to the inductive crank angle measurement system, the result of this work exhibits that torsional vibration has the most significant impacts on the crank angle measurement accuracy. Moreover, cylinder volume deformation has significant impact on the combustion parameters calculations.

- Considering all the discussed uncertainties, the crank angle measurement uncertainty in this work is deduced: 68.27% of the measurements have an uncertainty of ±0.14 CAD, while 99.73% of the measurements have an uncertainty of ±0.43 CAD. Moreover, with the crank angle measurement uncertainties, the IMEP uncertainty is also summarized as follows: 68.27% of the calculated IMEP have an uncertainty of ±0.33% and 99.73% of the calculated IMEP have an uncertainty of ±1%. Accordingly, for CA50 the uncertainty is [-1.2 -0.1] CAD.
- The pressure measurement shows significant impact on closed-loop pressure-based combustion control. Therefore, for advanced combustion control, those uncertainties need to be considered.
- The crank angle measurement uncertainties in this work do not indicate a significant impact on combustion control. However, for engines which have a larger number of cylinders, this can have a greater impact.

References

1. Hellen J., "Gas engine control based on integrated cylinder pressure measurement", Master's Thesis, Helsinki University of Technology, 2008.
2. Rebecchi P., "Fundamentals of thermodynamic for pressure-based low-temperature premixed diesel combustion control", Ph.D. Thesis, Institut für Verbrennungsmotoren und Kraftfahrwesen der Universität Stuttgart, 2013.
3. Rogers, D., “Engine Combustion: Pressure Measurement and Analysis,” (Warrendale, SAE International, 2010), doi:10.4271/R-388.
4. Shiqiao Q.; Zongsheng H.; and Xingshu W., "Optical Angular Encoder Installation Error Measurement and Calibration by Ring Laser Gyroscope," *IEEE Transactions on Instrumentation and Mesaurement* 59 (3):506-511, 2010, doi: 10.1109/TIM.2009.2022104.
5. Miljić, N., Popović, S., Kitanović M., "Engine Crankshaft Speed Measurement error Compensation," *MVM - Mobility Vehicle Mechanics* 41 (3):41-51, 2015.
6. Maurya R.K., Pal D.D., Agarwal A.K.,"Digital signal processing of cylinder pressure data for combustion diagnostics of HCCI engine," *Mechanical Systems and Signal Processing* 36(2013): 95-109, 2011, doi:10.1016/j.ymssp.2011.07.014
7. Davis, R. and Patterson, G., "Cylinder Pressure Data Quality Checks and Procedures to Maximize Data Accuracy," SAE Technical Paper 2006-01-1346, 2006, doi:10.4271/2006-01-1346.
8. Stank, J. D., "Analysis of in-cylinder pressure transducer data quality utilizing a SIDI turbocharged engine", Master's Thesis, Michigan Technological University, 2011.
9. Bueno Andre V., Velasquez Jose A. and Milanez Luiz F., "Internal Combustion Engine Indicating Measurements," Zahurul Haq Prof. (Ed.), InTech, http://www.intechopen.com/books/applied-measurement-systems/internal-combustion-engine-indicating-measurements, 2012, doi: 10.5772/37889.
10. Lee, S., Bae, C., Prucka, R., Fernandes, G. et al., "Quantification of Thermal Shock in a Piezoelectric Pressure Transducer," SAE Technical Paper 2005-01-2092, 2005, doi:10.4271/2005-01-2092.
11. Bertola A., Stadler J., Walter T., Wolfer P., C. et al., "Pressure sensors, Pressure indication during knocking conditions," Kistler Instruments AG, https://www.kistler.com/?type=669&fid=169&model=download 2006.
12. JCGM.,"Evaluation of measurement data-Guide to the expression of uncertainty in measurement," September 2008.
13. Accreditation, American Association for Laboratory, "G104 - Guide for Estimation of Measurement Uncertainty in Testing," December 4, 2014.
14. Daniel J.; Erik F.; Mattias K., "A flywheel error compensation algorithm for engine misfire detection," *Contron Engineering Practice* 47: 37-47, 2015, doi:10.1016/j.conengprac.2015.12.009.
15. Bucak, İ. Ö., "Position Error Compensation via a Variable Reluctance Sensor Applied to a Hybrid Vehicle Electric Machine," *Sensors* 10:1918-1934, 2010, doi: 10.3390/s100301918.
16. Lutowicz, M., "Unsteady Angular Speed of Diesel Engine Crankshaft Preliminary Examination," *KONES Powertrain and Transport* 19(4):394-399, 2012.
17. Farzin H. M., Ali F., "Stress Analysis and Optimization of Crankshafts Subject to Dynamic Loading," http://www.recycle-steel.org/~/media/Files/Autosteel/Programs/LongProducts/crankshaft_full_report_2.pdf, August 2007.
18. Stadler J., Ciecinski M., Wimmer A. et al., "Influence of Crankshaft Torsion on Cylinder Pressure Diagnostics," *MTZ Industrial* 5(1):58-65, 2015, doi:10.1007/s40353-015-0511-z.

Contact Information

Xiaoguo Storm
University of Vaasa, Vaasa, Finland
xxue@uwasa.fi

Acknowledgments

This work is sponsored by FLEXe and HERCULES-2 programs. Also the authors would like to thank to University of Vaasa for sponsoring and providing support for this work. Special thanks to the many dedicated technicians and engineers at Wärtsilä Finland Oy who have contributed the data and support that are needed in this work.

Definitions/Abbreviations

ASE - signal average envelope

USE - signal upper envelopes

LSE - signal lower envelopes

CA50 - crank angle position where 50% of heat is released

STD - standard deviation

HRR - heat release rate

THR - total heat release

CHR - cumulative heat released

FSO - full scale output

DWT - Dead-weight Tester

CAD - crank angle degree

PP - peak pressure

LPP - location of peak pressure

IMEP - indicated mean effective pressure

GUM - guide for measurement uncertainty

FMEP - friction mean effective pressure

V - cylinder volume

P - cylinder pressure

K - specific heat ratio

Vs - cylinder swept pressure

The Engineering Meetings Board has approved this paper for publication. It has successfully completed SAE's peer review process under the supervision of the session organizer. The process requires a minimum of three (3) reviews by industry experts.

ISSN 0148-7191

http://papers.sae.org/2017-01-1067